Journal of Atmospheric and Terrestrial Physics, Vol. 50, No. 9, pp. 819–829, 1988.
Printed in Great Britain.

0021–9169/88 $3.00+ .00

Formation of mesospheric VHF echoing layers due to a gravity wave motion

YOSHIKAZU MURAOKA
Department of Physics, Hyogo College of Medicine, Nishinomiya, Hyogo 663, Japan

TAKUYA SUGIYAMA
Department of Physics, Kyoto University, Kyoto 606, Japan

KOHJI KAWAHIRA
Toyama National College of Technology, Toyama, Toyama 939, Japan

and

TORU SATO, TOSHITAKA TSUDA, SHOICHIRO FUKAO and SUSUMU KATO
Radio Atmospheric Science Center, Kyoto University, Uji, Kyoto 611, Japan

(*Received in final form* 13 *June* 1988)

Abstract—We present mesospheric backscattered VHF echo power and wind velocity data indicating the co-existence of a threefold strongly echoing layer and a wave motion, observed on 20 September 1985 with the MU radar at Shigaraki (34.9°N, 136.1°E), Japan. The echoing layers are clearly connected with the vertical and horizontal wind perturbations due to the wave. The analysis of the wind data have shown that the wave motion is due to an internal inertia–gravity wave with the vertical and horizontal wavelengths of 6 and 400 km, respectively, and period of 5.6 h. Evaluating the atmospheric stability in the wave field with the estimated wave parameters, the echoing layers are shown to be consistent with statically stable regions generated by the wave. It is suggested from our results that Fresnel scattering is a dominant echoing mechanism for a VHF radar beam in the mesosphere, as well as in the lower stratosphere.

1. INTRODUCTION

Recently it has been demonstrated by a number of workers that sensitive VHF radars can be used to investigate the dynamics of the middle atmosphere (e.g. BALSLEY and GAGE, 1980; RÖTTGER, 1980; GAGE and BALSLEY, 1984; FRITTS and RASTOGI, 1985; KATO *et al.*, 1986; RÖTTGER, 1987a). This technique uses radar echoes arising from refractive index fluctuations in the middle atmosphere and in the lower ionosphere. Analysis of these echoes enables the measurements of the dynamic property of the atmosphere—winds, waves and, under certain circumstances, dynamic and static stabilities. An excellent review of the recent results obtained with the VHF radars is given by RÖTTGER (1987a). The echoing mechanisms that give rise to the signals observed on VHF radars has been considered to be mainly due to turbulent scatter and Fresnel (partial) reflections (e.g. BALSLEY and GAGE, 1980; RÖTTGER, 1980). The evidence of Fresnel reflection from the troposphere and stratosphere, in addition to scattering, has been pointed out by GAGE and GREEN (1978) and by RÖTTGER and LIU (1978). GAGE *et al.* (1981, 1985) proposed a Fresnel scattering model which accounted for observed stratospheric echo power profiles quite well. In this model, the received power depends upon the vertical gradient of a generalized atmospheric refractive index, assuming that the radar beam is scattered in a volume filled with stable laminae (cf. HOCKING and RÖTTGER, 1983).

In the mesosphere, RÖTTGER *et al.* (1979) have discussed the role of Fresnel reflection on a typical structure of observed echo profiles. However, the echoing mechanism is still an unresolved problem although the feature of mesospheric echoes has been investigated in the course of a number of observational studies (see reviews by RÖTTGER, 1987a). The mesospheric echoes show a remarkable seasonal variation (BALSLEY *et al.*, 1983; CZECHOWSKY and RÜSTER, 1985). BALSLEY *et al.* (1983) have suggested that the echoes arise from a breakdown of tides and gravity waves. This may be an indication that the turbulence generation by the wave breaking is responsible for the scattering of the radar beam. SMITH *et al.* (1986) have also claimed that the enhancement of

mesospheric echoes is associated with a statically unstable region induced by a gravity wave motion. However, these results are not consistent with the findings of RÜSTER and KLOSTERMEYER (1985) and YAMAMOTO *et al.* (1987) that echo power maxima may be associated with dynamical instabilities generated in the maximum shear regions of gravity waves. Furthermore, it has been proposed that heavy water cluster ions play an important role on the enhancement of mesospheric echoes (KELLY and ULWICK, 1988). Thus, the dynamical conditions which lead to the reflection and/or to the scattering of VHF signal are not yet fully understood in the mesosphere.

In this paper, we first describe significant observational results concerning the profile of VHF echo intensity in the mesosphere, which were obtained by using the MU (middle and upper atmosphere) radar operated by Radio Atmospheric Science Center at Shigaraki, Japan. It is now being established that the MU radar can provide reasonably high spatial and temporal resolution data on atmospheric motions and turbulent intensities (KATO *et al.*, 1986; FUKAO *et al.*, 1986; MURAOKA *et al.*, 1987). Our purpose here is to discuss a posssible cause of the formation of mesospheric VHF echoing layers, considering some features of the atmosphere disturbed by gravity wave motions.

2. MU RADAR EXPERIMENTS

The middle and upper atmosphere (MU) radar at Shigaraki (34.9°N, 136.1°E), Japan is now fully operational, with all 475 yagis and 1 MW peak power. Details of the system and experimental results may be found in the papers of FUKAO *et al.* (1985a,b) and KATO *et al.* (1986). Main parameters of the MU radar on our observations carried out on 20 September 1985 are summarized in Table 1. To measure three components of wind velocity in the mesosphere, the main beam of the MU radar was transmitted in the vertical and two off-vertical (northward and southward by 10° from the zenith) directions, in turns. The received echo signals were sampled at intervals of 600 m in the height range of 60–97.8 km and were coherently integrated over 20 pulses of transmission. The signals were transformed into power spectra by using the 128 point FFT. After we removed the effect of meteor echoes observed intermittently above 85 km (see TSUDA *et al.*, 1985 for the behaviour of meteor echoes), we determined the radial wind velocities using a nonlinear, least square fitting method of the Doppler shifted spectrum data which were incoherently accumulated for about 30 min. Meridional and zonal components of the mesospheric wind velocity were derived from the radial velocities considering the vertical component. The average of the four successive wind profiles was estimated as a mean profile for about 2 h and was smoothed by applying a three point running mean to remove small scale noise. Furthermore, the contribution of large scale components with a vertical scale larger than about 20 km, which are due to the background mean flow, tides and so on, was estimated by applying a low pass filter with respect to height.

Table 1. Main parameters of the MU radar on our observations

Parameter	Value
Radar frequency	46.5 MHz
Peak power	1 MW
Beam width	3.6°
Height range	60–97.8 km
Height resolution	600 m
Time resolution	208 s

3. THEORETICAL BACKGROUNDS OF GRAVITY WAVE AND ATMOSPHERIC STABILITY

In this section, we describe several relations used in our data analysis, which are derived from the theories of gravity wave propagation in the middle atmosphere and atmospheric stability. The theory of gravity waves and their breaking has been well developed by a number of workers (e.g. GOSSARD and HOOKE, 1975; LINDZEN, 1981; FRITTS, 1984; FRITTS and RASTOGI, 1985). We consider adiabatic inviscid gravity wave motions with intrinsic frequencies ω such that:

$$f \leqslant \omega \ll N_0 \tag{1}$$

in a mean state atmosphere in hydrostatic balance. Here, f is the inertial frequency and N_0 is a mean Brunt–Väisälä frequency defined by:

$$N_0^2(z) \equiv (g/\bar{\theta})\bar{\theta}_z, \tag{2}$$

where $\bar{\theta}$ and g are the mean potential temperature and the acceleration due to gravity, respectively, and the subscript denotes differentiation. We may assume the wave motions to occur in an x–z plane with a mean velocity $\bar{u}(z)$ in the x-direction. Note that the x-axis is taken in accordance with the direction of horizontal wave propagation which is arbitrary in the real atmosphere. Thus, we now assume that the perturbations in the equations of motion have solutions of the form:

$$\psi = \psi_0(z)\, e^{z/2H} \exp[ik(x-ct)+imz]. \tag{3}$$

Here k and m are the horizontal and vertical wave numbers, respectively, c is the phase velocity of the wave motion, and H is the scale height of the mean atmosphere ($H = \kappa g/N_0^2$). By using the Doppler shifted frequency $\sigma = kc$ observed in the mean flow $\bar{u}$, note that ω is defined as:

$$\omega \equiv \sigma - k\bar{u}. \tag{4}$$

For our purpose, it is reasonable to assume that the mean static stability N_0^2 is slowly varying with height and that $m \gg H$. Provided further that the wave motions themselves are hydrostatic, we see that the equations of motion yield a dispersion relation:

$$m^2 = \frac{k^2 N_0^2}{\omega^2 - f^2}. \tag{5}$$

Then, we find from the momentum equation that a polarization relation between the horizontal components of perturbation wind velocity is given by:

$$v' = -(if/\omega)u'. \tag{6}$$

We also see from the continuity equation that:

$$w' = -(k/m)u' \tag{7}$$

and from the adiabatic energy equation that:

$$\theta' = [i\bar{\theta}_z/m(c-\bar{u})]u'. \tag{8}$$

Dynamical and convective instabilities, which are considered to contribute to the generation of turbulence in the middle atmosphere, have been investigated theoretically from a viewpoint of the stability of the atmosphere disturbed by gravity wave motions (HODGES, 1967; LINDZEN, 1981; see also reviews by FRITTS and RASTOGI, 1985). The principal measure of stability, as the buoyancy effects of the density gradient over-ride its inertial effects, is the Richardson number:

$$Ri \equiv N^2/(u_z^2 + v_z^2), \tag{9}$$

where

$$N^2 = (g/\theta)\theta_z \tag{10}$$

denotes the total static stability of the atmosphere with the total potential temperature, i.e. $\bar{\theta} + \theta'$. A detailed discussion on the significance of a local Richardson number in a wave field is given by GOSSARD and HOOKE (1975). The theory states that the necessary condition for dynamical instability is $Ri < 1/4$. If Ri becomes negative owing to a gravity wave motion, i.e.

$$N^2 < 0, \tag{11}$$

the wave field is considered to be convectively unstable (HODGES, 1967; LINDZEN, 1981). LINDZEN (1981) have further indicated that turbulence in the middle atmosphere arises from the unstable breakdown of gravity waves.

Assuming that $c - \bar{u}$ are slowly varying with height, the derivative of (8) with respect to z may be approximated as:

$$\theta_z' \fallingdotseq \frac{-\bar{\theta}_z}{c-\bar{u}}u'. \tag{12}$$

Thus, we see from (2), (10) and (12) that:

$$N^2 = N_0^2\left(1 - \frac{u'}{c-\bar{u}}\right). \tag{13}$$

The expression (13) indicates that the horizontal velocity perturbation in the direction of propagation achieves a maximum at the level where the wave motion has the smallest static stability. Note that the upward velocity perturbation also attains a maximum at this level taking account of $m < 0$ for internal modes considered here. Using (13), the condition (11) is rewritten as:

$$\left(1 - \frac{u'}{c-\bar{u}}\right) < 0. \tag{14}$$

Neglecting the vertical shear of the mean flow, the local Richardson number (9) in a wave field, as determined by wave and mean flow quantities, can be written in terms of the real perturbation variables as:

$$Ri = \frac{\{1 - [u_0/(c-\bar{u})]\cos\phi\}[1 - (f/\omega)^2]}{[u_0/(c-\bar{u})]^2[\sin^2\phi + (f/\omega)^2\cos^2\phi]}, \tag{15}$$

where we have written

$$Re\,[u'] = u_0\cos\phi \tag{16}$$

and u_0 and ϕ are the amplitude of the wave and the phase function:

$$\phi = kx + mz - \sigma t. \tag{17}$$

Thus, we may estimate the local Richardson number in a wave field as well as the static stability if the wave parameters and mean flow quantities are already known from observation. Before doing this, it may be significant to examine the change of Ri in an idealized gravity wave field quantitatively. In Fig. 1, the value of Ri estimated with (15) is plotted as function of ϕ for waves with various f/ω. If the amplitude of vertically propagating wave comes to be so large as to satisfy the condition (14) because of the exponential growth with height, it is evident from Fig. 1(a) that the wave field becomes convectively unstable around the level corresponding to $\phi = 0$. The minimum Richardson number is achieved at the phase, where the total static

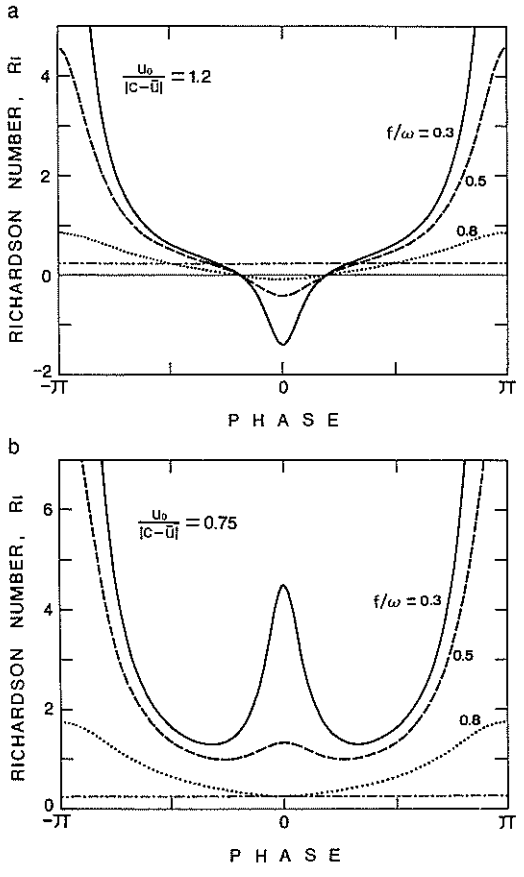

Fig. 1. Plots of local Richardson number (Ri) as a function of phase in internal inertia–gravity wave motions with various frequencies (f/ω). The wave amplitudes are larger in panel (a) and smaller in panel (b) than that required for convective instability. The criterion for dynamical instability ($Ri = 1/4$) is shown by a dot–dashed line.

stability N^2, is also a minimum and the upward velocity perturbation is a maximum. Note that the wave field is dynamically unstable at the levels which adjoins to the convectively unstable region. On the other hand, if (14) is not satisfied owing to the insufficient growth of wave amplitude, the region corresponding to $\phi \sim 0$ is rather stabilized for waves with relatively high frequency in those considered here (i.e. for $f/\omega \to 0$), as shown in Fig. 1(b). This is because the vertical shear of the horizontal wind velocity perturbation is almost zero at $\phi = 0$ and N^2 remains positive though this value attains its minimum at that phase level. Thus, the maxima and minima of Ri are seen twice, respectively, during the phase change of a wavelength when the wave field is still stable around $\phi \sim 0$.

4. RADAR DATA ANALYSIS

Figure 2 shows a comparison between the mesospheric echo intensity and wind velocity measured with the MU radar during the period of 1430–1635 LT on 20 September 1985. In Fig. 2a, the time–height contour of echo intensity for the VHF beam in the vertical direction is compared with the height profile of an averaged vertical wind velocity during this period. Time–height contours of echo intensity in two other off vertical directions and the corresponding height profiles of averaged meridional and zonal wind velocities are also shown in Figs. 2b and c, respectively. Each echo contour shows that a threefold intense echoing layer was seen around the heights of 70, 76 and 82 km during the observation. These altitudes were almost constant while the intensity changed with time. This indicates that these layers existed stably for a long time in a large horizontal extent. The most intense echo was observed at the middle layer and the weakest one was from the highest layer (cf. Fig. 5a). Each averaged wind profile clearly shows a wave motion with the vertical wavelength of 6 km in the background mean flow. Note that the echoing layers correspond to the wave induced downward and northward wind velocity perturbations with a phase difference.

In Fig. 3, the change in the averaged wind velocity with height is shown by two hodograms for the zonal–meridional and meridional–vertical components. Figure 3a shows that the horizontal component of wind velocity perturbation rotates clockwise with increasing height, indicating the downward phase progression (i.e. $m < 0$) of an internal gravity wave mode transporting its energy and momentum upward. Figure 3b shows that the downward and northward components of the velocity perturbation are well correlated with each other. Taking the x-axis in the southward direction and considering $m < 0$, we see from (7) that the observed wave propagated almost southward in the horizontal direction. This is justified from the direction of the major axis in elliptic polarization of the horizontal wind perturbation (Fig. 3a). We may estimate further from (7) that the horizontal wavelength ($\lambda_h = 2\pi/k$) turns out to be 400 km with the vertical wavelength ($\lambda_z = 2\pi/m$) of 6 km and $w'/u' \sim 0.015$ obtained from Fig. 3b.

We have shown in Fig. 2 that the strongly echoing layers had hardly changed their altitudes during the observation. The altitudes corresponded to a phase of the wave motion observed simultaneously. If the wave is as stationary ($\sigma \sim 0$) as lee waves observed sometimes in the lower stratosphere, the phase becomes a function of height alone at the point of observation.

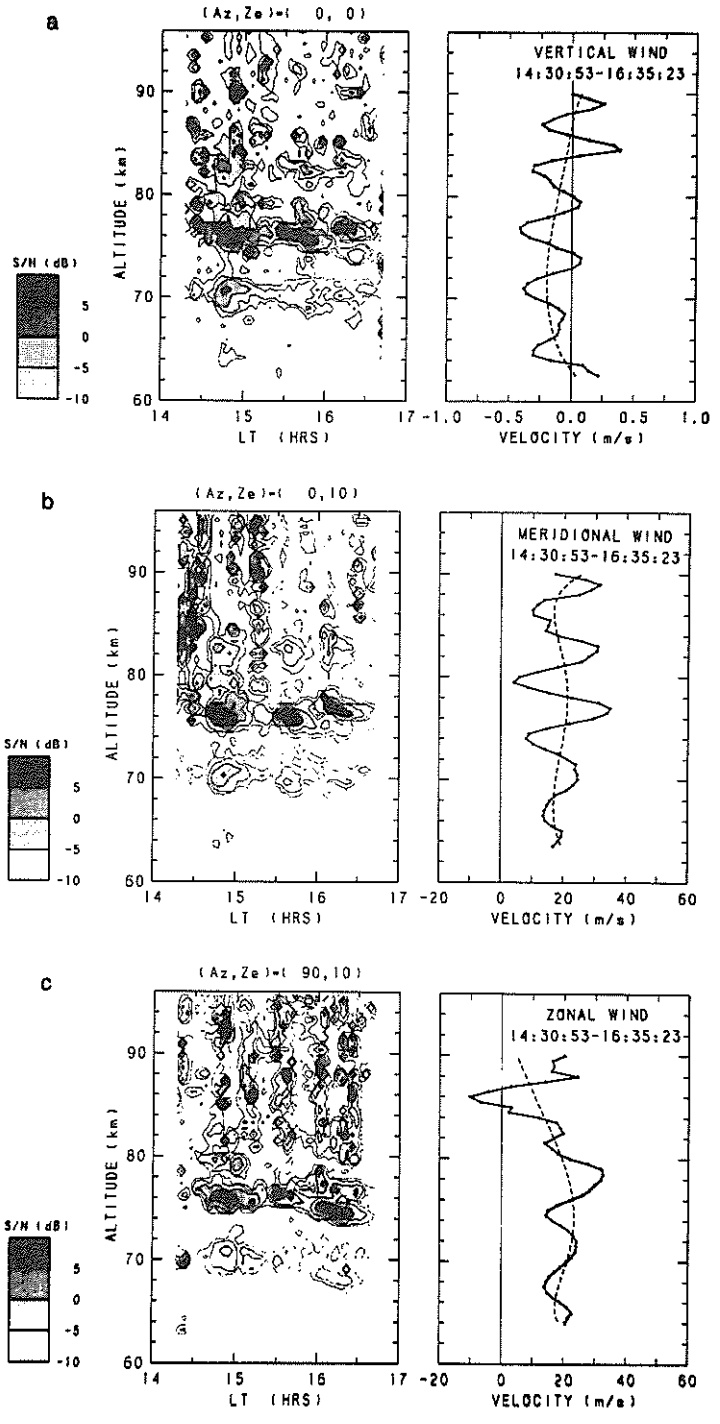

Fig. 2. (a) Time–height contour of mesospheric echo intensity in the vertical radar beam (left) and averaged profile of the vertical component of wind velocity (right) observed in the period of 1430–1635 LT on 20 September 1985. The contour levels are given at 5 dB intervals. The positive value of the wind velocity indicates an upward motion. The dashed curve indicates a background mean flow. (b) Echo intensity in the beam deflected northward by 10° from the zenith and meridional component wind profile. The positive value of the wind velocity indicates a northward motion. (c) Echo intensity in the beam deflected eastward by 10° from the zenith and zonal component wind profile. The positive value of the wind velocity indicates an eastward motion.

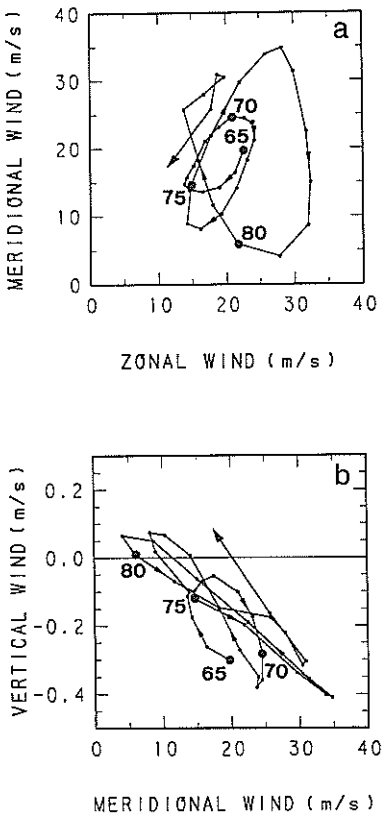

Fig. 3. Hodograms showing polarization of the wind velocity perturbation shown in Fig. 2, in (a) zonal–meridional and (b) meridional–vertical planes. The altitudes at which the wind velocity is measured are indicated in km units at 5 km intervals.

Thus, we may regard the wave as stationary if the echo structure arises from the wave motion. Then, we estimate from (4) that the intrinsic frequency of the wave motion:

$$\omega \fallingdotseq -k\bar{u} = -2\pi\bar{u}/\lambda_h \sim 3.1\times10^{-4}\,\mathrm{s}^{-1} \qquad (18)$$

and then the period,

$$T = 2\pi/\omega \fallingdotseq -\lambda_h/\bar{u} \sim 5.6\,\mathrm{h} \qquad (19)$$

with $\bar{u} \sim -20\ \mathrm{m\,s^{-1}}$ near 75 km height from Fig. 2b. Note that we define southward wind as $u > 0$ here. We also see that $f/\omega \sim 0.27$ with $f = 8.3\times10^{-5}\ \mathrm{s^{-1}}$ at 34.9°N. This ratio is shown to be almost the same order ($\sim$0.3) as is estimated directly from the elliptic polarization of horizontal perturbation wind near 75 km in Fig. 3a, considering that the direction of the major axis in the elliptic polarization changes above 77 km height. Thus, we can safely say that the observed wave was almost stationary in the northward mean flow (cf. Fig. 2b).

Using (5) with the observed values of $\bar{u} \sim -20\ \mathrm{m\,s^{-1}}$ and $\lambda_z \sim 6$ km near 75 km height (cf. Fig. 2b), we see that the Brunt–Väisälä frequency in the mesosphere was:

$$N_0 \fallingdotseq m\omega/k \fallingdotseq -2\pi\bar{u}/\lambda_z \sim 0.021\,\mathrm{s}^{-1} \qquad (20)$$

since $(f/\omega)^2 \ll 1$. This indicates that the observed wave motion is due to an inertia–gravity wave (i.e. $N_0 \gg \omega \geqslant f$). Furthermore, we see that the scale height of the mean atmosphere was $H = \kappa g/N_0^2 \sim 6.2$ km with $\kappa = 2/7$ and $g = 9.6\ \mathrm{m\,s^{-2}}$ near 75 km height and then the mean mesospheric temperature was 210 K. These values agree reasonably well, for example, with those at 75 km height in the U.S. Standard Atmosphere, 1976. Here we note that the vertical wavelength of the observed wave varied slowly with height (Fig. 2b). The change is clearly seen in Fig. 5c. The wavelength became shorter by degrees with increasing height. As suggested from (5), this is due to a gradual increase of N_0^2 with height and also implies a monotonous temperature decrease. This is an atmospheric property in the mesosphere.

Figure 4 is another example showing the existence of a gravity wave motion and the related echoing layers, which were observed during the period of 1202–1406 LT on 20 September 1985. It is shown in this figure that the vertical wavelength of the wave motion was also 6 km although it was disturbed by small scale noise. The other wave parameters were almost the same as those of the wave motion shown in Fig. 2, except for a slight difference in the direction of horizontal propagation. The enhanced echoes were observed around the heights of 70, 76 and 82 km and these heights were consistent with the regions indicating the wave induced downward and northward wind perturbations with a phase difference. The observed echo was most intense in the middle layer and became weaker in the highest one (cf. Fig. 6a).

We now proceed to estimate the atmospheric stability in the observed wave field by using the measured wind velocity and the estimated wave parameters. Then, we compare the calculated Richardson number and static stability with the measured echo intensity. Such a comparison is shown in Fig. 5. Figure 5a shows a height profile of echo power averaged for the contour shown in Fig. 2a. In Fig. 5b, two height profiles for the estimated Richardson number are shown. Substituting (13) into (9) the Richardson number is rewritten in terms of the already known parameters from the observation as:

$$Ri = \frac{N_0^2[1-u'/(c-\bar{u})]}{(u_z^2+v_z^2)}. \qquad (21)$$

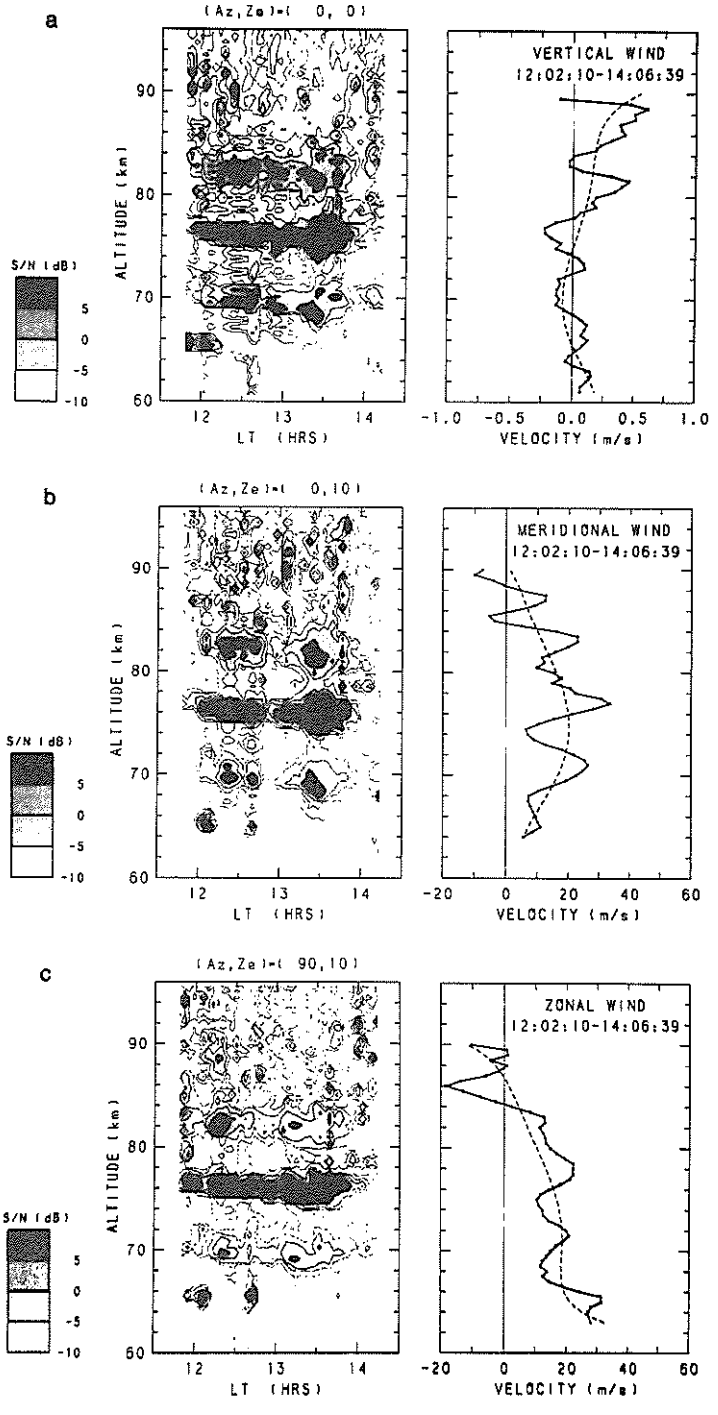

Fig. 4. Same as Fig. 2 except for observation during the period of 1202–1406 LT on 20 September 1985.

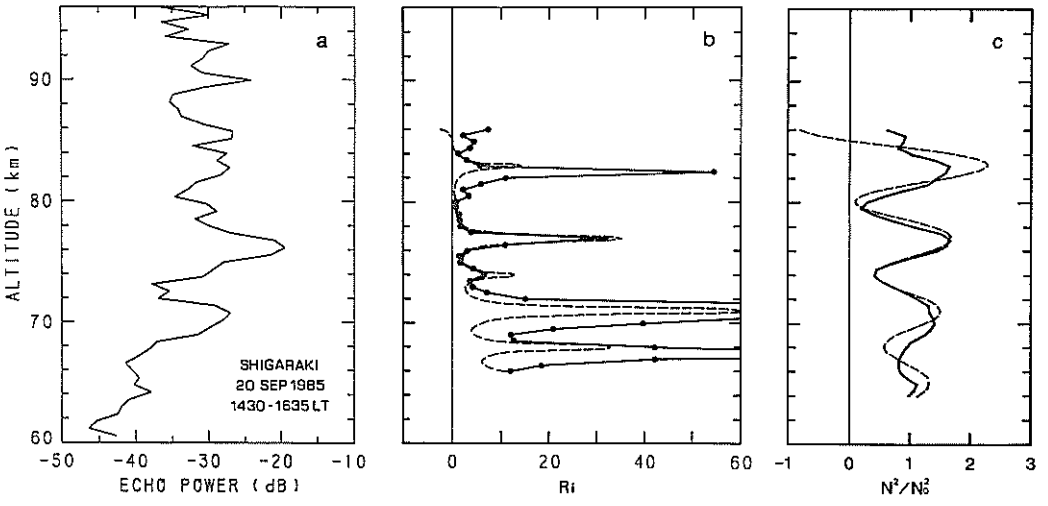

Fig. 5. Comparison between height profiles of (a) an averaged echo power for the vertical beam shown in Fig. 2a, (b) estimated local Richardson number (Ri) and (c) normalized total static stability (N^2/N_0^2). The solid lines in the panels (b) and (c) indicate the height changes of Ri and N^2/N_0^2 estimated with parameters of the observed wave as shown in Fig. 2. The dotted curves indicate the height changes for a modeled wave with an exponential growth rate.

The solid line in Fig. 5b shows a height change in the Richardson number estimated from (21) with (20) and the measured wind velocity. The dashed curve represents a height change in the Richardson number estimated from (15) with the wave parameters estimated in the preceding paragraphs, assuming a wave with an exponential growth with height. These two height changes agree well with each other except for the lower heights, as is expected. The difference in the lower heights is partly due to the small amplitude of wave and partly due to a phase difference between the model and actual wave (cf. Fig. 5c). It is evident from Fig. 5b that the wave field was not dynamically and convectively unstable below 84 km since the Richardson number did not become smaller than 1/4. Note that the Richardson number became very small ($Ri \sim 0.8$) around 80 km because of the wave growth with height. Above this altitude, the estimated Richardson number is larger than that expected from the exponentially growing wave. This indicates that the wave field has been stabilized above 80 km, in reality, because of a wave dissipation. The dissipation is clearly seen as an attenuation of the wave amplitude above 80 km in the wind profiles shown in Figs. 2b and c. Thus, it is evident that the stabilization of the wave field is a result of the wave dissipation. It is also noted that the elliptic polarization in the horizontal wind velocity shown in Fig. 3a apparently breaks down around 82 km. Since the Richardson number anticipated from the non-dissipating wave motion is very small around 80 km, the wave breaking may be connected with dynamical or convective instability in the wave field.

It is important to note in Fig. 5b that the observed echoing layers are associated with the wave induced stable regions (maxima of Ri corresponding to $\phi \sim \pi$ in Fig. 1b). These stable regions are situated around 71, 77 and 83 km as shown in Fig. 5b. Note that each height of the stable regions is lower by about 1 km than that of the corresponding echoing layer. The measured echo became weak around the heights corresponding to another maxima of Ri ($\phi \sim 0$ in Fig. 1b). Note that the wave field would be unstable at this phase level if the wave amplitude were sufficiently large (cf. Fig. 1a). Thus, it appears that the echoing layer is not associated with the occurrence of instability in the wave field.

To clarify the association between the echoing layers and the atmospheric stability, we further compare the averaged echo intensity profile with a height change in the total static stability of the atmosphere shown in Fig. 5c. The solid line in this figure shows a height change in the normalized total static stability estimated from (13) with the measured wind velocity. The dashed curve indicates a change in the total static stability anticipated from an exponentially growing gravity wave with the same parameters as estimated in this section. The comparison between Figs. 5a and c clearly show that the echoing layers are associated with the regions indicating an increase of the

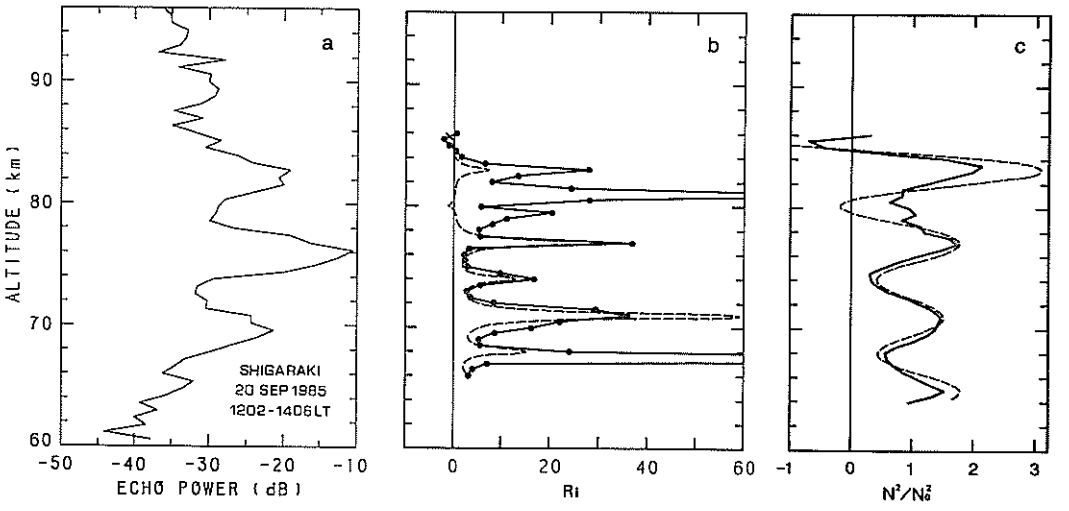

Fig. 6. Same as Fig. 5 except for comparison between height profiles concerning data shown in Fig. 4.

total static stability as a result of the wave motion. Note that the echo intensity in the highest layer around 82 km, became relatively weak in comparison with the other layers. This is probably due to the reduction of the total static stability due to the wave breaking as shown in Fig. 3a.

Figure 6 shows another comparison between an averaged height profile of the mesospheric echo intensity shown in Fig. 4a and height changes in the Richardson number and total static stability of the atmosphere disturbed by the wave motion shown in Fig. 4. The solid line in Fig. 6c indicates a height change of the normalized static stability estimated from (13) with the measured wind velocity. The dashed curve indicates a height change expected from an exponentially growing gravity wave with the same parameters as estimated in this section. These changes agree well with each other as is expected. It is noted that the atmosphere disturbed by the wave is being restored to its original state ($N^2 \rightarrow N_0^2$) above 80 km, as a result of the wave breaking due to the occurrence of convective instability ($N^2 < 0$) around 80 km. The wave breaking is seen typically in the meridional wind profile in Fig. 4b. It is clear from the comparison between Figs. 6a and c that the echoing layers corresponded to the regions indicating an increase of the total static stability due to the wave motion with a phase difference. It is noted that the enhancement of observed echo has no direct relation to the occurrence of convective instability in the wave field. Rather, the enhancement was weakened above the breaking level. Thus the weak enhancement in the highest layer seems to be due to the reduction of the total static stability as a result of the wave breaking shown in Fig. 4b.

5. SUMMARY AND DISCUSSION

We here consider a possible cause of the appearance of VHF echoing layers, summarizing our observational results obtained with the MU radar. The results have shown threefold strongly echoing layers in the mesosphere. At the same time, the heights are consistent with regions showing the downward and northward wind perturbations due to a wave motion with the vertical wavelength of 6 km. The wave motion has been shown to be due to an internal mode of inertia–gravity waves ($N_0 \gg \omega \geqslant f$). Our results further show that the wave was almost stationary ($\sigma \sim 0$). This has been endorsed by the fact that the heights of the echoing layers hardly changed during the observation. Thus, there is little doubt that the appearance of the echoing layers are associated closely with the gravity wave motion.

The observed stationary gravity wave may be a result of the vertical propagation of lee wave forced topographically in the troposphere, as suggested by LINDZEN (1981) and HOLTON (1982). Such lee waves have been occasionally observed in the stratosphere with VHF radars (RÜSTER and KLOSTERMEYER, 1983). RÖTTGER (1987b) have discussed a possible connection of mesospheric echo structure with very long period inertia–gravity waves, taking account of the wave induced shear and temperature change. It is well known that such long period waves are observed occasionally in the mesosphere (BALSLEY *et al.*, 1983; SMITH *et al.*, 1986; YAMAMOTO *et al.*, 1987). SMITH *et al.* (1986) have indicated that the enhanced mesospheric echoes are seen at heights where the wave field becomes most statically unstable (i.e. negative

temperature lapse rate). This scenario is consistent with the wave breaking theory that the turbulence generation process is due to the unstable breakdown of tides and gravity waves (LINDZEN, 1981). The connection with instabilities has been also pointed out by BALSLEY *et al.* (1983). On the other hand, it has been indicated that the enhanced echo is associated with a maximum shear generated by waves, which may lead to dynamical instability (RÜSTER and KLOSTERMEYER, 1985; YAMAMOTO *et al.*, 1987). In our measurements as shown in Figs. 5 and 6, the enhancement of mesospheric echoes was seen just below heights where the static stability shows a maximum. Therefore, there is a possibility that the echoing layers are connected with regions indicating minima of Ri (cf. Figs. 5b and 6b). Although these minima are related to the maxima of the vertical shear of the horizontal wind component ($\phi = \pm\pi/2$ in Fig. 1b), it should be noted that the minima of Ri are seen twice in the vertical range of a wavelength. However, the observed echo enhancement was seen only once in the one wavelength height range. Furthermore, the observed wave field did not become dynamically unstable ($Ri < 1/4$) below 80 km. Thus, it appears that the enhanced echoes in our measurements are not connected directly with dynamically unstable regions generated by the long period inertia–gravity wave.

We have also shown that values of the mean atmosphere such as temperature can be derived reasonably from the dispersion relation (5) with the estimated wave parameters, where the wave propagates without any dissipation. This indicates that the wave parameters are estimated self-consistently. Estimating the atmospheric stability in the wave field with these parameters and the directly measured wind velocity, we have pointed out that the observed echoing layers are consistent with the statically stable regions rather than with the convectively unstable regions generated by the long period gravity wave. According to a Fresnel scattering model (GAGE *et al.*, 1981; 1985), the enhanced echo obtained at vertical incidence by VHF radars is attributed to Fresnel reflection from multiple thin layers showing strong gradient of refractive index under conditions of stable stratification. By applying this model in the stratospheric observation, GAGE *et al.* (1985) have given a good explanation of the vertical profiles of VHF echo power observed in the stratosphere. In this model, the power reflection coefficient for transmitted pulse depends upon the refractivity structure determined by the vertical gradient of stratospheric potential temperature. This is why the dry air contributions to the refractive index is most important in the stratosphere (e.g. BALSLEY and GAGE, 1980; RÖTTGER, 1980). However, free electrons become the major contributing factor in the mesosphere where the concentration increases rapidly with height (cf. HOCKING, 1985). Here, it is interesting to recall that the observed echoing layers were associated with the wave induced downward wind perturbation. The transport of electron, ions and neutral species by the vertical wind can influence the vertical profile of electron density through the complicated chemical reaction in the D-region if the wave period is appropriately long (e.g. BRASSEUR and SOLOMON, 1986). This process is mainly controlled by the attachment of an electron with a neutral species with a long chemical lifetime. Thus, it is suggested that the vertical transport of D-region chemical species by the gravity wave brings about a considerable change in the vertical gradient of the radio refractive index in the mesosphere. Finally, we refer to the phase difference between the echoing layers and the perturbation wind field. Since the chemical lifetime of neutral species related to the electron loss process in the D-region is comparable to the period of the observed wave, it is expected that the change in the electron density has a time lag for the wave field. The time lag may be observed as the phase difference in the vertical direction in the stationary wave field. This problem will be resolved by using a D-region chemical model in the near future. At present, we do not know the reason why the enhanced echo is observed in the mesosphere. However, it is apparent that the echoing layers in our observation are primarily associated with the statically stable regions, which have been generated by the long period inertia–gravity wave observed simultaneously.

6. CONCLUSIONS

In this paper we have examined the features of mesospheric echo structure and wind velocity profiles observed with the MU radar at Shigaraki, Japan. The echo contour profile has shown a threefold echoing layer existing continually in the mesosphere. The altitudes were almost constant during the observation and were consistent with a phase of the wind velocity fluctuations. The fluctuations have shown the vertical propagation of an internal inertia–gravity wave with the vertical and horizontal wavelengths of 6 and 400 km, respectively, and the period of 5.6 h. It is evident from our analysis that the echoing layers were formed in connection with the vertically propagating gravity wave. Estimating further the stability of the atmosphere disturbed by the gravity wave motion, we have shown that the echoing layers are consistent with

regions indicating the increase of total static stability due to the wave motion. This suggests that a plausible cause of the enhanced echoes is a Fresnel scattering from a volume filled with stable laminae of radio refractive index, as has been proposed by GAGE *et al.* (1981, 1985). In the mesosphere, however, free electrons are most important for the contribution to the refractive index (e.g. HOCKING, 1985). Therefore, it is expected that the electron profile is modified through the vertical transport of *D*-region chemical species by the long period gravity wave.

Acknowledgements—We thank the staff of Shigaraki MU Observatory for their help with the observations. One of the authors (Y.M.) also thanks Prof. T. SATO and Dr. H. MURATA of the Hyogo College of Medicine for useful discussion and encouragement. The MU radar belongs to, and is operated by, the Radio Atmospheric Science Center of Kyoto University.

REFERENCES

BALSLEY B. B. and GAGE K. S.	1980	*Pure Appl. Geophys.* **118,** 452.
BALSLEY B. B., ECKLUND W. L. and FRITTS D. C.	1983	*J. atmos. Sci.* **40,** 2451.
BRASSEUR G. and SOLOMON S.	1986	*Aeronomy of the Middle Atmosphere.* D. Reidel, Dordrecht.
CZECHOWSKY P. and RÜSTER R.	1985	*Handbook for MAP* **18,** 207.
FRITTS D. C.	1984	*Rev. geophys. Space Phys.* **22,** 275.
FRITTS D. C. and RASTOGI P. K.	1985	*Radio Sci.* **20,** 1247.
FUKAO S., SATO T., TSUDA T., KATO S., WAKASUGI K. and MAKIHIRA T.	1985a	*Radio Sci.* **20,** 1155.
FUKAO S., TSUDA T., SATO T., KATO S., WAKASUGI K. and MAKIHIRA T.	1985b	*Radio Sci.* **20,** 1169.
FUKAO S., SATO T., TSUDA T., YAMAMOTO M. and KATO S.	1986	*J. atmos. terr. Phys.* **48,** 1269.
GAGE K. S. and GREEN J. L.	1978	*Radio Sci.* **13,** 991.
GAGE K. S. and BALSLEY B. B.	1984	*J. atmos. terr. Phys.* **46,** 739.
GAGE K. S., BALSLEY B. B. and GREEN J. L.	1981	*Radio Sci.* **16,** 1447.
GAGE K. S., ECKLUND W. L. AND BALSLEY B. B.	1985	*Radio Sci.* **20,** 1493.
GOSSARD E. E. and HOOKE W. H.	1975	*Waves in the Atmosphere.* Elsevier, New York.
HOCKING W. K.	1985	*Radio Sci.* **20,** 1403.
HOCKING W. K. and RÖTTGER J.	1983	*Radio Sci.* **18,** 1312.
HODGES R. R. JR	1967	*J. geophys. Phys.* **72,** 3455.
HOLTON J. R.	1982	*J. atmos. Sci.* **39,** 791.
KATO S., TSUDA T., YAMAMOTO M., SATO T. and FUKAO S.	1986	*J. atmos. terr. Phys.* **48,** 1259.
KELLEY M. C. and ULWICK J. C.	1988	*J. geophys. Res.* **93,** 7001.
LINDZEN R. S.	1981	*J. geophys. Res.* **86,** 9707.
MURAOKA M., KAWAHIRA K., SATO T., TSUDA T., FUKAO S. and KATO S.	1987	*Geophys. Res. Lett.* **14,** 1154.
RÖTTGER J.	1980	*Pure Appl. Geophys.* **118,** 494.
RÖTTGER J.	1987a	*Phil. Trans. R. Soc.* **A323,** 611.
RÖTTGER J.	1987b	*Adv. Space Res.* **7,** 345.
RÖTTGER J. and LIU C. H.	1978	*Geophys. Res. Lett.* **5,** 357.
RÖTTGER J., RASTOGI P. K. and WOODMAN R. F.	1979	*Geophys. Res. Lett.* **6,** 617.
RÜSTER R. and KLOSTERMEYER J.	1983	*Geophys. astrophys. Fluid Dynamics* **26,** 107.
RÜSTER R. and KLOSTERMEYER J.	1985	*Handbook for MAP* **18,** 216.
SMITH S. A., FRITTS D. C., BALSLEY B. B. and PHILBRICK C. R.	1986	*Handbook for MAP* **20,** 136.
TSUDA T., YAMAMOTO M., SATO T. and KATO S.	1985	*Radio Sci.* **20,** 1241.
YAMAMOTO M., TSUDA T., KATO S., SATO T. and FUKAO S.	1987	*J. geophys. Res.* **92,** 11993.